

Phase diagram of the interacting persistent spin-helix state

Hong Liu¹, Weizhe Edward Liu², Stefano Chesi³, Robert Joynt⁴, and Dimitrie Culcer¹

¹*School of Physics and Australian Research Council Centre of Excellence in Low-Energy Electronics Technologies,*

UNSW Node, The University of New South Wales, Sydney 2052, Australia

²*School of Physics and Astronomy and Australian Research Council Centre of Excellence in Low-Energy Electronics Technologies,*

Monash Node, Monash University, Melbourne 3800, Australia

³*Beijing Computational Science Research Center, Beijing 100193, China*

⁴*Department of Physics, University of Wisconsin-Madison, Madison, Wisconsin 53706, USA*

 (Received 4 May 2020; revised 27 October 2020; accepted 29 October 2020; published 10 November 2020)

We study the phase diagram of the interacting two-dimensional electron gas (2DEG) with equal Rashba and Dresselhaus spin-orbit coupling, which for weak coupling gives rise to the well-known persistent spin-helix phase. We construct the full Hartree-Fock phase diagram using a classical Monte Carlo method analogous to that used in *Phys. Rev. B* **96**, 235425 (2017). For the 2DEG with only Rashba spin-orbit coupling, it was found that at intermediate values of the Wigner-Seitz radius r_s , the system is characterized by a single Fermi surface with an out-of-plane spin polarization, whereas at slightly larger values of r_s , it undergoes a transition to a state with a shifted Fermi surface and an in-plane spin polarization. The various phase transitions are first order, and this shows up in discontinuities in the conductivity, and the appearance of anisotropic resistance in the in-plane polarized phase. In this paper we show that the out-of-plane spin-polarized region shrinks as the strength of the Dresselhaus spin-orbit interaction increases and entirely vanishes when the Rashba and Dresselhaus spin-orbit coupling strengths are equal. At this point the system can be mapped onto a 2DEG without spin-orbit coupling, and this transformation reveals the existence of an in-plane spin-polarized phase with a single displaced Fermi surface beyond $r_s > 2.01$. This is confirmed by classical Monte Carlo simulations. We discuss experimental observation and useful applications of the novel phase as well as caveats of using the classical Monte Carlo method.

DOI: [10.1103/PhysRevB.102.205410](https://doi.org/10.1103/PhysRevB.102.205410)

I. INTRODUCTION

The two-dimensional electron gas (2DEG) with spin-orbit coupling (SOC) and many-body electron-electron interactions is a paradigmatic system in semiconductor physics and technology in addition to being one of the fundamental models in condensed-matter physics. Much of the interest in SOC centers around the fact that it enables spin generation, spin manipulation, and spin detection without using external magnetic fields or magnetic materials [1,2], whereas at the same time being manifest in a great variety of spin textures in solids [3–5], many of which are associated with topological effects [6–8], unconventional states of matter [9,10], and novel phases [1,11–20]. Acquiring a full understanding of the spin-orbit coupled 2DEG is key to our ability to utilize the electron spin degree of freedom in semiconductors to control the spin states and transfer spin information, which is a fundamental requirement for future spintronic devices and quantum computing [21–25] among other applications.

Keeping in mind both basic science and potential technological interest, identifying many-body ground states with novel spin textures and polarizations is one of the goals of present-day condensed-matter research. This problem is notoriously difficult analytically even in the absence of SOC. The Hartree-Fock (HF) method often provides simple analytical

solutions, and though it entirely ignores the effect of correlations it generally provides useful insights into the structure of the single-particle levels [26–28]. In addition to this, the past few decades have seen dramatic improvements in our ability to simulate complicated physical systems using Monte Carlo (MC) approaches [29–35].

This paper investigates the possibility of broken-symmetry states with complex spin patterns in the two-dimensional electron liquid with SOC. There is good but not complete understanding of the polarized phases of the electron fluid without SOC [4,11,36,37]. In the three-dimensional (3D) case, there is the possibility of a partially polarized phase [36], whereas for the 2D case there is no evidence for a stable partially polarized phase, and the transition from unpolarized to polarized is first order [11]. Furthermore, calculations at intermediate densities are difficult because very small energy differences are important and any approximation has to treat the various phases of the gas with equal accuracy [38].

The situation becomes even more complicated in spin-orbit coupled 2DEGs. In nonmagnetic materials where inversion symmetry is broken but time-reversal invariance remains intact, strong SOC may play the role of an effective magnetic field that locks electron spins with their momenta yielding complex textures. These broken-symmetry states are strongly suggested by the existence of chiral spin modes coupled to

plasmons by the SOC which are already present in the symmetric Fermi-liquid (FL) state [39,40]. In general the SOC in semiconductor 2DEGs can take several forms. In realistic semiconductor nanostructures both the Rashba and the Dresselhaus SOC are often present. Rashba SOC is present primarily because quantum wells frequently have a built-in asymmetry [41] and has been experimentally observed in semiconductor heterostructures where it has been proved to be tunable in strength by means of a gate voltage [42–44]. The Dresselhaus SOC reflects the inversion asymmetry inherent in zinc-blende lattices, which includes the crystal structure of many III–V and II–VI semiconductors, such as GaAs, InSb, and CdTe [45]. In 2DEGs the SOC can be described by an effective momentum-dependent magnetic field. This effective field favors spin textures that have zero net moment, whereas the electron-electron interactions favor ferromagnetism. This gives rise to a multitude of phases, many of which remain to be explored in detail. An insightful theoretical approach adopted in earlier studies of interacting spin-orbit coupled systems involved applying a unitary transformation to leading order in the spin-orbit strength, which yields a transformed Hamiltonian whose eigenstates are also spin and angular momentum eigenstates [46,47]. More recently it has been shown that in addition to the well-known out-of-plane spin-polarized (OP) phase [13,48], the interacting 2DEG with Rashba spin-orbit coupling exhibits an in-plane spin-polarized (IP) phase with a shifted Fermi surface [49], somewhat resembling a Pomeranchuk instability. It is caused by an exchange enhancement of the current-induced spin polarization. The phase transition from the OP phase to the IP phase was shown to be first order. This IP phase appears already at intermediate values of r_s , the Wigner-Seitz radius, which represents the relative strength of the electron-electron interactions to the average kinetic energy. The IP phase is likewise expected in systems with Dresselhaus SOC since the Rashba and Dresselhaus interactions are related by a spin rotation. Several additional recent works have examined the interplay between Rashba SOC and electron-electron interactions in 2DEGs [12,14,50].

Motivated by these observations we examine the phase diagram of the interacting 2DEG as we change the ratio of the Rashba and Dresselhaus spin-orbit interactions, focusing on systems with nearly equal Rashba and Dresselhaus SOC [51–54]. The system with exactly equal Rashba and Dresselhaus interactions is an interesting special case with SU(2) symmetry. This symmetry is robust against spin-independent disorder and interactions and is generated by operators whose wave vector depends on the coupling strength. It renders the spin lifetime infinite at this wave vector, giving rise to a persistent spin helix [52,54,55], which has been realized experimentally [51–53]. When the Rashba and Dresselhaus interactions are of equal magnitude, the effective magnetic field describing the spin-orbit interaction singles out a well-defined direction in momentum space. There is a single spin-quantization axis, and all the spins in the system point either parallel or antiparallel to this axis. In this paper we determine the full HF phase diagram of the 2DEG with equal Rashba and Dresselhaus interactions.

When either the Rashba or the Dresselhaus interaction is dominant we expect the same phase diagram as in Ref. [49],

whereas the case when the two interactions are equal is qualitatively different. Experimentally, the phase transitions are observed in transport properties, most notably the DC conductivity. We present analytical results for the phase diagram in the case when the two SOC strengths are equal and perform classical MC simulations along the lines of Ref. [49], focusing on the zero-temperature properties of the electron gas. Our analytical calculations reveal that the out-of-plane spin-polarized phase in Fig. 4 shrinks as the magnitudes of the Rashba and Dresselhaus interactions approach each other, i.e., as the persistent spin helix state is approached. When the Rashba and Dresselhaus SOC are equal the out-of-plane phase disappears altogether and only an in-plane spin-polarized phase exists for all $r_s > 2.01$. It is characterized by a single Fermi surface, which is displaced from the Brillouin zone center and has a nontrivial spin texture, which becomes more pronounced at higher values of r_s and of the spin-orbit interaction strength. Our expectations based on this analytical treatment are confirmed by classical MC simulations, which rely on the same method as that used in Ref. [49].

We find, however, two caveats related to the application of the classical MC method to this system. First, in a narrow parameter regime the *bare* MC phase diagram appears to display a phase with a small out-of-plane spin polarization, which we have referred to as OP* throughout this paper. To determine whether this phase is physical or not we varied the number of points in the MC simulations and studied the evolution of the ground state in this region as a function of the number of k -points N . We have found that in the thermodynamic limit $N \rightarrow \infty$ the ground state has an in-plane spin polarization in exact agreement with the analytical calculations. The energy difference, whereas larger than the numerical error, remains relatively small. Second, the persistent spin helix system exhibits a spin-density wave phase that is degenerate with the in-plane spin-polarized phase and that is not captured accurately by our MC method. The existence of this phase can be determined by analytical arguments, and we believe it is related to the appearance of the OP* phase in the MC phase diagram. The application of the classical MC depends on using a class of HF wave functions for which the ground-state energy can be reduced to a classical minimization problem. The method will not find ground states outside this class, such as the spin-density wave.

The Hohenberg-Mermin-Wagner theorem has recently been extended to show that itinerant ferromagnetism does not exist at any finite temperature for strictly two-dimensional electron liquids without SOC or other terms that break the SU(2) spin rotation symmetry [56]. In the presence of SOC, the existence of such ordering remains an open question. Our results are obtained in mean-field theory and, therefore, shed no light on this issue (although they point up its urgency).

The organization of this paper is as follows: In Sec. II, we describe the Hamiltonian of the system and the spin texture as well as the phase diagram obtained from analytical arguments using a gauge transformation. In Sec. III, the phase diagram of the interacting 2DEG with equal Rashba and Dresselhaus SOC is given by our classical MC simulation. In Sec. IV, we compare the results obtained from the two preceding sections and discuss the possibilities for experimental observation. In Sec. V, we summarize our results.

II. HAMILTONIAN AND GAUGE TRANSFORMATION

The general many-body Hamiltonian is written as

$$H_{\alpha,\beta} = \sum_{kss'} \langle ks | H_{\alpha,\beta}^{(0)} | ks' \rangle c_{k,s}^\dagger c_{k,s'} + V^{ee}, \quad (1)$$

where $c_{k,s}$ is the annihilation operator for a single electron with wave-vector k and spin index $s = \pm$ and $c_{k,s}^\dagger$ is the corresponding creation operator. Here we consider a translationally invariant system, which is permissible as long as localization effects are negligible. Hence, only diagonal matrix elements in k appear in the single-particle Hamiltonian (first term). Including both Rashba (α) and Dresselhaus (β) spin-orbit SOC, $H_{\alpha,\beta}^{(0)}$ reads

$$H_{\alpha,\beta}^{(0)} = \frac{\hbar^2 k^2}{2m} + \alpha(k_y \sigma_x - k_x \sigma_y) + \beta(k_x \sigma_x - k_y \sigma_y), \quad (2)$$

where σ_i 's are Pauli matrices and m is the effective mass. The electron-electron interaction V^{ee} is as follows:

$$V^{ee} = \frac{1}{2A} \sum_{kk'ss'} \sum_{q \neq 0} V_q c_{k+q,s}^\dagger c_{k'-q,s'}^\dagger c_{k's'} c_{ks}, \quad (3)$$

where A is the area of the system. The specific form of V_q is not important for the arguments developed in this section as long as V^{ee} has the usual coordinate representation $V^{ee} = \sum_{i<j} V(r_i - r_j)$ [which is the case for Eq. (3)]. In later evaluations we will make use of the screened 2D Coulomb interaction represented by the following matrix element:

$$V_q = \frac{e^2}{2\epsilon_r \epsilon_0 (k_{\text{TF}} + |q|)}, \quad (4)$$

in which q denotes the momentum transfer, k_{TF} is the Thomas-Fermi wave number, and ϵ_r is the static dielectric constant.

We now specialize Eq. (1) to the main case of interest in this paper with equal Rashba and Dresselhaus coefficients ($\alpha = \beta$). In this limit, we simplify the notation and drop the reference to the Dresselhaus coupling (i.e., $H_\alpha \equiv H_{\alpha,\alpha}$ and $H_\alpha^{(0)} \equiv H_{\alpha,\alpha}^{(0)}$). It is also convenient to perform a change in coordinates and rewrite the single-particle Hamiltonian Eq. (2) as

$$H_\alpha^{(0)} = \frac{\hbar^2 (\tilde{k}_x^2 + \tilde{k}_y^2)}{2m} - 2\alpha \tilde{k}_x \tilde{\sigma}_y, \quad (5)$$

where $\tilde{k}_x = (k_x + k_y)/\sqrt{2}$ and $\tilde{k}_y = (k_y - k_x)/\sqrt{2}$ are rotated by $\pi/4$ with respect to the original coordinates and the spin operators $\tilde{\sigma}_{x,y}$ defined in a similar manner ($\tilde{\sigma}_z = \sigma_z$). Importantly, the natural spin quantization axis is along a fixed direction $e_{\tilde{y}} = (e_y - e_x)/\sqrt{2}$, which is independent of k . The single-particle spectrum is immediately obtained as

$$\epsilon_{0,k\pm} = \frac{\hbar^2 (k \mp q_\alpha)^2}{2m} - 2m\alpha^2, \quad (6)$$

where $q_\alpha = \frac{\sqrt{2}\alpha m}{\hbar^2} (e_x + e_y)$. Note that the $\pm q_\alpha$ shift in momentum appearing in Eq. (6) gives rise to two distinct Fermi surfaces displaced in opposite directions.

Besides the existence of the conserved quantity $\tilde{\sigma}_y$, it was recognized early on that a spatially dependent spin rotation,

$$U_\alpha = \exp \left[i \frac{m\alpha}{\hbar^2} (\sigma_y - \sigma_x)(x + y) \right] \quad (7)$$

relates the noninteracting Hamiltonian $H_\alpha^{(0)}$ to the familiar case without SOC, and this is still true after including spin-independent potentials [54,57]. The many-body form of U_α acts as $U_\alpha c_{k,s} U_\alpha^\dagger = c_{k+sq_\alpha,s}$ and commutes with the electron-electron interaction. Therefore, the whole family of many-body Hamiltonians H_α , obtained by setting $\alpha = \beta$ in Eq. (1), may be related to the extensively studied 2D electron liquid without SOC [58]. Explicitly,

$$H_\alpha = U_\alpha (H_{\alpha=0}) U_\alpha^\dagger - 2N_e \frac{m\alpha^2}{\hbar^2}, \quad (8)$$

where N_e is the total number of electrons.

A. Spin-polarized states

Many properties of the spin-orbit coupled system can be obtained directly from the exact mapping (8), but here we will be mainly interested in the occurrence of a spontaneous spin polarization. It is then useful to consider the spin-density operators $\tilde{S}(r) = \sum_i \tilde{\sigma}_i \delta(r - r_i)$, where $i = 1, \dots, N_e$ labels the electrons and $\tilde{\sigma}$'s are the rotated Pauli matrices introduced after Eq. (5). U_α transforms the spin-polarization operators as follows:

$$U_\alpha \tilde{S}_x(r) U_\alpha^\dagger = \tilde{S}_x(r) \cos 2q_\alpha r + \tilde{S}_z(r) \sin 2q_\alpha r, \quad (9)$$

$$U_\alpha \tilde{S}_z(r) U_\alpha^\dagger = \tilde{S}_z(r) \cos 2q_\alpha r - \tilde{S}_x(r) \sin 2q_\alpha r, \quad (10)$$

whereas $U_\alpha \tilde{S}_y(r) U_\alpha^\dagger = \tilde{S}_y(r)$. The above transformation shows that, whenever the system at $\alpha = 0$ has a spin-polarized ground state, the corresponding many-body state with $\alpha \neq 0$ is a collective spin wave where the \tilde{x}, \tilde{z} components of the spin-polarization process in space. In other words, whereas at $\alpha = 0$ the Stoner transition leads to ferromagnetism, a sufficiently strong electron interaction with $\alpha \neq 0$ leads to the spontaneous formation of spin-density waves.

A case of particular interest is the uniform polarization along $e_{\tilde{y}}$, which is left unchanged by the transformation U_α . Due to the SU(2) symmetry, it is always possible to choose the spin polarization along this particular direction. Then, not only the phase boundaries at $\alpha = 0$ and $\alpha \neq 0$ (with respect to, e.g., the electron density) are the same, but also the spin polarization is unchanged by the presence of SOC.

The difference between the two scenarios (with and without SOC) becomes clear by considering the full set of states generated by the SU(2) group. When $\alpha = 0$, we can find a suitable spin rotation $R_{\hat{n}}$ which rotates the uniform spin polarization from $e_{\tilde{y}}$ to any desired direction \hat{n} . The corresponding symmetry operation with $\alpha \neq 0$ is $U_\alpha R_{\hat{n}} U_\alpha^\dagger$ which, applied to the uniformly polarized state, will generate a nontrivial spin wave with the same energy. Thus, the Stoner transition indeed corresponds to the spontaneous formation of a collective persistent spin-helix state.

B. Paramagnetic phase

The paramagnetic phase is apparently less interesting as there is no spin polarization. However, the existence of persistent spin-helix states is reflected in the quasiparticle excitations. We first note that, without spin-orbit coupling, the spin-degenerate Fermi surface survives the effect of the

interactions (Luttinger's theorem [58]). Applying U_α to the interacting state without spin-orbit coupling leads to two distinct Fermi surfaces, centered around $\pm q_\alpha$. Such as for the noninteracting case [see Eq. (6)], the two Fermi surfaces correspond to orthogonal spin directions \pm along $\tilde{\sigma}_y$.

Without spin-orbit interaction, low-lying excited states have $k \simeq k_F$ close to the Fermi wave-vector ($k_F = \sqrt{2\pi n}$, where n is electron density) and arbitrary spin direction, specified by the usual polar angle θ and the azimuthal angle ϕ . For $\alpha \neq 0$, we should transform the electron creation operator $\cos(\theta/2)c_{k,+}^\dagger + e^{i\phi} \sin(\theta/2)c_{k,-}^\dagger$ through U_α . Since $U_\alpha c_{k,s} U_\alpha^\dagger = c_{k+sq_\alpha,s}$, we obtain

$$c_{k,\hat{n}}^\dagger \equiv \cos(\theta/2)c_{k+q_\alpha,+}^\dagger + e^{i\phi} \sin(\theta/2)c_{k-q_\alpha,-}^\dagger, \quad (11)$$

where \hat{n} gives the direction of the spin when $\alpha = 0$. Equation (11) allows us to define stable quasiparticles $c_{k,\hat{n}}^\dagger|F\rangle$ on top of the (interacting) ground-state $|F\rangle$.

From the previous discussions, especially Eqs. (9) and (10), it is clear that the quasiparticles states $c_{k,\hat{n}}^\dagger|F\rangle$ carry a spatially processing spin polarization. In fact, the form of Eq. (11) involves a coherent superposition of states at both Fermi surfaces (except for $\theta = 0$), and the $\pm q_\alpha$ displacements induce the formation of a spin-wave with wave-vector $2q_\alpha$. For a Fermi liquid, the lifetime of the $c_{k,\hat{n}}^\dagger|F\rangle$ states becomes infinite in the limit $k \rightarrow k_F$. This shows that in the paramagnetic phase the natural excitations of the system are interacting spin-helix states.

C. Mean-field approximation

With the help of the $c_{k,\hat{n}}^\dagger$ operators, we can also give a mean-field description of the Stoner transition with spin-orbit interaction. The paramagnetic phase corresponds to

$$|F\rangle \simeq \prod_{k \leq k_F} c_{k,\hat{n}}^\dagger c_{k,-\hat{n}}^\dagger |0\rangle, \quad (12)$$

where the choice $\hat{n} = e_{\tilde{y}}$ is perhaps more natural, but any other direction of \hat{n} is equivalent: They all give the same spin-unpolarized ground state of the noninteracting Hamiltonian. On the other hand, the mean-field spin-polarized states can be written as

$$|F\rangle \simeq \prod_{k \leq \sqrt{2}k_F} c_{k,\hat{n}}^\dagger |0\rangle, \quad (13)$$

which actually depend on the direction \hat{n} , reflecting the broken SU(2) symmetry. As discussed, only when $\hat{n} = e_{\tilde{y}}$ the spin density is uniform. For other orientations, all the electrons occupy spin-helix states, and the spin density is processing in space as described by Eqs. (9) and (10). It is oriented along \hat{n} only at periodic positions along the $e_{\tilde{x}}$ direction (e.g., \hat{n} can be taken as the polarization direction at $r = 0$).

For the unscreened Coulomb interaction, the phase diagram of the electron liquid at a fixed ratio β/α depends on two dimensionless parameters (e.g., r_s and $\tilde{\alpha}$, defined below). The Wigner-Seitz radius r_s is

$$r_s = \frac{me^2}{4\pi\epsilon_r\epsilon_0\hbar^2\sqrt{\pi n}}, \quad (14)$$

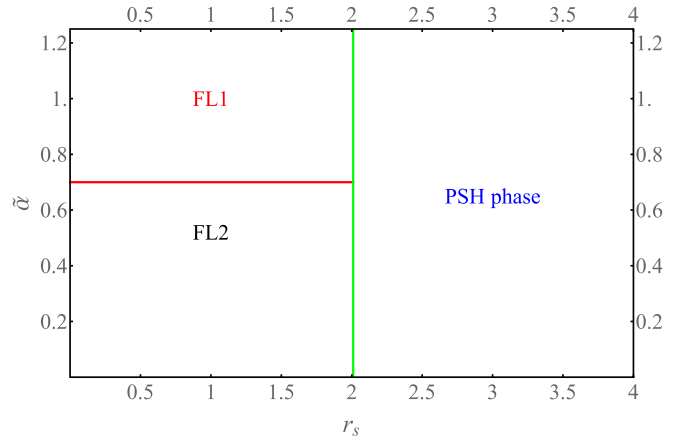


FIG. 1. Phase diagram of a 2D electron liquid with Rashba equal to Dresselhaus SOC in the HF approximation obtained by gauge transformation. It shows the results of an exact mapping to the case of no SOC followed by a HF calculation of the diagram. Here, $\tilde{\alpha}$ and r_s are dimensionless measures for the strength of Rashba (Dresselhaus) SOC and electron-electron interactions, respectively. For the paramagnetic Fermi-liquid phases FL1 and FL2, there is no net spin polarization. The states of the PSH phase are spin-density waves analogous to the persistent spin helix. Only the state with in-plane polarization along $e_{\tilde{y}}$ has a uniform spin density.

and is a measure of the interaction strength [58]. Instead, α and β can be rescaled as follows [49]:

$$\tilde{\alpha} = \frac{m\alpha}{\hbar^2\sqrt{\pi n}}, \quad \tilde{\beta} = \frac{m\beta}{\hbar^2\sqrt{\pi n}}. \quad (15)$$

Here, $\tilde{\alpha}$ ($\tilde{\beta}$) is a measure of the Rashba (Dresselhaus) SOC relative to the kinetic energy. Although for $\beta = 0$ the dependence of the phase boundaries on $\tilde{\alpha}$ is nontrivial [49], when $\alpha = \beta$ we find from Eq. (8) that the phase boundaries should be independent of $\tilde{\alpha}$. They are simply given by the values in the absence of spin-orbit interaction.

The differences between these two cases can be seen clearly by comparing their phase diagrams. The analytical phase diagram for $\alpha = \beta$, shown in Fig. 1, reflects the physics discussed above. In the paramagnetic region $r_s < 2.01$, we also mark the FL1 region $\tilde{\alpha} > 1/\sqrt{2}$ in which the $s = \pm$ Fermi disks become nonoverlapping (obtained from the condition $|q_\alpha| > k_F$). This is a single-particle transition whose position is also unaffected by electron interactions, according to the discussion at the beginning of Sec. II B. The result of MC simulations for the $\alpha = \beta$ case will be presented in the next section. Meanwhile, in Fig. 2 we reproduce the the HF mean-field phase diagram for $\beta = 0$ [49], where the transition to the OP and IP states (respectively, with in-plane and out-of-plane spin polarization) depend on $\tilde{\alpha}$ in a complicated way.

Finally, we comment on the expectation value of the total momentum operator $P = \sum_i p_i$ in the collective persistent spin-helix state giving

$$\frac{1}{mN_e} \langle F|P|F\rangle = \frac{\hbar q_\alpha}{m} \cos \theta. \quad (16)$$

Except for $\theta = \pi/2$, there is a finite expectation value of P along $e_{\tilde{x}} = (e_x + e_y)/\sqrt{2}$, reflecting a displaced

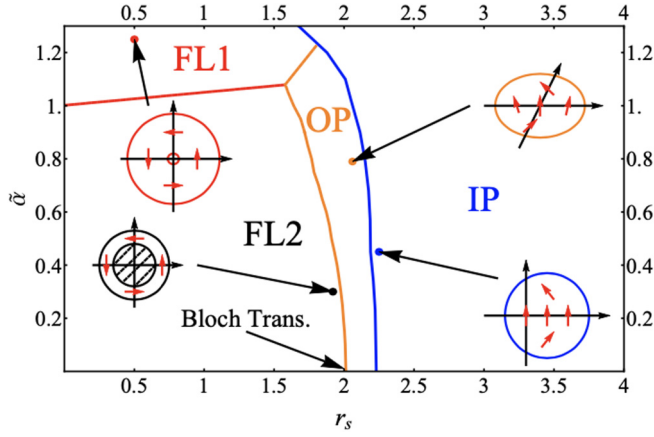


FIG. 2. Phase diagram of a2D electron liquid with Rashba SOC obtained by solving the HF equations using a MC method from Ref. [49]. Here, $\tilde{\alpha}$ and r_s are dimensionless measures for the strength of Rashba SOC and electron-electron interactions, respectively: $\tilde{\alpha}$ corresponds to the ratio of the Fermi wavelength and spin-precession length, and r_s is the Wigner-Seitz radius of the 2D electron system. The distinguishing ground-state features for each individual phase are indicated schematically. For the paramagnetic Fermi-liquid phase FL1 (FL2), there is no net spin polarization, and the ground state is a Fermi sea formed from one (both) spin subband(s). In contrast, the OP phase is characterized by a centered Fermi surface and an out-of-plane magnetization. The IP phase is the most unconventional, exhibiting an in-plane magnetization associated with a shifted Fermi sea.

momentum-space occupation of the spin-polarized states. The displacement is largest when the polarization is uniform and oriented along $\tilde{\sigma}_y$ ($\theta = 0$). As usual, Eq. (16) does not imply a finite current in equilibrium since the single-particle velocity along $e_{\tilde{x}}$ is given by $\tilde{p}_x/m - 2\alpha\tilde{\sigma}_y/\hbar$. The finite expectation value of P/mN_e is exactly canceled by the contribution to the velocity from the spin polarization,

$$\frac{2\alpha}{\hbar n} \langle F | \tilde{S}_y(r) | F \rangle = \frac{2\alpha}{\hbar} \cos \theta. \quad (17)$$

Note from Eqs. (9) and (10) that $\langle F | \tilde{S}_y(r) | F \rangle = n \cos \theta$ is the only component of the spin-polarization density which is independent of r . Although the above properties are most easily verified by using $|F\rangle$ in Eq. (13), they are also valid beyond the mean-field approximation.

III. MONTE CARLO SIMULATION OF INTERACTING 2DEG WITH RASHBA AND DRESSSELHAUS SPIN-ORBIT COUPLINGS

A. Total energy of 2DEG with spin-orbit coupling

In the statically screened HF approximation, the exchange energy of the system can be written as

$$E_{\text{ex}} = -\frac{1}{L^2} \sum_{k \neq k'} \frac{e^2 [\tilde{s}_k \cdot \tilde{s}_{k'} + n_k n_{k'}]}{4\epsilon_0(k_{\text{TF}} + |k - k'|)}, \quad (18)$$

where f_k is the density matrix in equilibrium, whereas $n_k = \frac{1}{2} \text{Tr} f_k$ and $\tilde{s}_k = \frac{1}{2} \text{Tr} (\sigma f_k)$ are the electron's occupation number and net spin polarization at k , respectively. The total

energy can be expressed as

$$E_{\text{tot}} = \text{Tr} [f_k H_{\alpha,\beta}^{(0)}] + E_{\text{ex}}. \quad (19)$$

We assume that the screening effect is negligible due to the low electron density, so $k_{\text{TF}} = 0$. In the following subsections we use the same method as in Ref. [49] to find the minimum-energy configuration. When r_s is close to a phase boundary, the total energy is linearly dependent on r_s , which allows us to use a linear fitting to determine the transition points.

This approach is appropriate for addressing generic values of α and β . On the other hand, Eq. (19) assumes a uniform ground state and cannot capture the inhomogeneous spin-density waves of the phase separated hydrocarbons (PSH) phase. This is not a severe limitation as the PSH phase includes a uniform state, polarized on the plane of the 2DEG. When $\alpha \neq \beta$, the SU(2) symmetry is broken and the system should allow an IP phase, instead of the PSH phase. In fact, a prominent IP phase was discussed in Ref. [49] with $\beta = 0$. Following these remarks, in this section we will prefer the denomination IP phase, keeping in mind that when $\alpha = \beta$ the IP and PSH phases come to coincide.

Furthermore, the system can also sustain a phase with OP polarization [49]. In general, we find that all transitions, except the essentially single-particle FL1-FL2 transitions, are first-order. That the FL-OP transition is first order is expected from classic results on the ferromagnetism of the system with SOC, and our simulations also show this. The OP-IP phase transition is also expected to be first order since the residual symmetry groups of the two phases do not satisfy an inclusion relationship. Our results are also consistent with this.

B. Phase diagram of 2DEG with $\tilde{\alpha} \neq 0$ and $\tilde{\beta} = 0$

Using a MC simulation, we reproduce the result for 2DEG with only Rashba SOC in Fig. 2 in Ref. [49]. As r_s increases, the interaction becomes more effective, producing a tendency towards ferromagnetism. When $\tilde{\alpha} = 0$ there is the classic Bloch transition that occurs at $r_s = 2.01$.

There are two conventional FL states with one and two occupied spin subbands, respectively. The only effect of the exchange interaction is to renormalize upwards the strength of the Rashba term, and there is no net spin polarization for the two Fermi liquid states. The phase boundary of the two Fermi-liquid states is well described by the (noninteracting) critical density equation $n_c = \frac{m^2 \alpha^2}{\pi \hbar^3}$.

As r_s increases with finite $\tilde{\alpha}$, the ferromagnetic phase is modified to the OP phase which is shown in Fig. 3 where spins have a z component and a component along the effective field due to the Rashba spin-orbit coupling. At small k , they point nearly along the z direction, but as k increases, they follow the spin-orbit-induced field. When r_s is even larger, the right half of the phase diagram is the IP phase. The key feature of the IP phase is that the spin polarization is completely in-plane and the IP phase does not have any symmetry on the Fermi surface, even though both of them only have a single band.

C. Phase diagram of 2DEG with $\tilde{\alpha} = \tilde{\beta}$

In this subsection, we take both Rashba and Dresselhaus SOC into account and set them to have equal strength. We

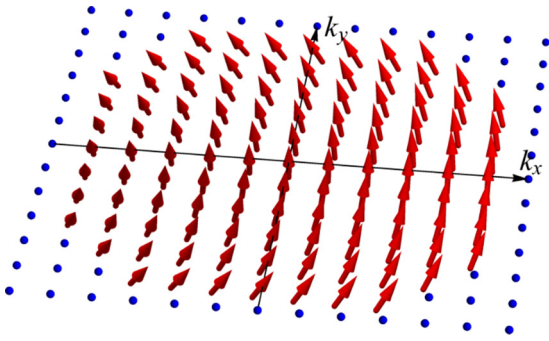


FIG. 3. The OP phase at $\tilde{\alpha} = 0.3$ and $r_s = 2.02$ in a 3D view. The OP phase comprises a single band with a circular Fermi surface and nontrivial out-of-plane spin polarization. Its in-plane spin polarization cancels out after summing over all the occupied states [49].

find four phases and plot the phase diagram as functions of $\tilde{\alpha}$ and r_s in Fig. 4. The number of k points is $N = 997$. The FL2 and FL1 phases [see Fig. 5] are the conventional FL states. The only effect of the Coulomb exchange interaction is to renormalize upwards the strength of the spin-orbit coupling. The FL state minimizes the single-particle energy by using the noninteracting states and occupation numbers.

When $r_s > 2.01$, the MC simulation shows that there is a narrow region which has partially out-of-plane spin polar-

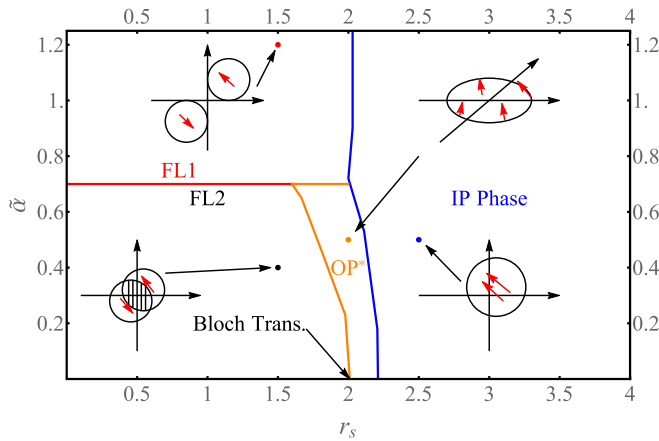


FIG. 4. Phase diagram of a 2D electron liquid with equal Rashba and Dresselhaus SOCs, obtained by solving the HF equations using a MC simulation. It shows the result of a numerical HF calculation, which should give the same result as Fig. 1, but due to numerical uncertainty, instead shows also the possibility of the OP* phase. Here, $\tilde{\alpha}$ and r_s are dimensionless measures for the strength of Rashba spin-orbit coupling and the electron-electron interactions, respectively: $\tilde{\alpha}$ corresponds to the ratio of the Fermi wavelength and spin-precession length, and r_s is the Wigner-Seitz radius of the 2D electron system. The distinguishing features for each individual phase are indicated schematically by giving a picture that shows the spin texture. Each such picture is connected by an arrow to its point in the actual parameter space. For the Fermi-liquid phases FL1 and FL2, there is no net spin polarization. In contrast, the OP* phase is characterized by an out-of-plane magnetization. However, it is believed to be an artifact of the finite size of the system. The IP phase exhibits an in-plane magnetization associated with a shifted Fermi sea and because of the SU(2) symmetry is equivalent to the PSH phase of Fig. 1.

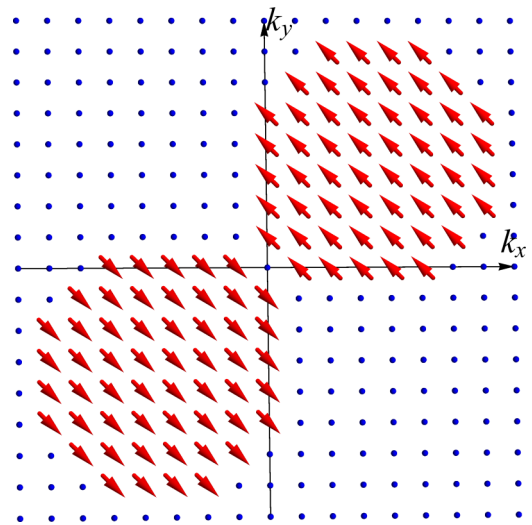


FIG. 5. The FL1 at $\tilde{\alpha} = \tilde{\beta} = 0.81$, $r_s = 1.65$ in a 3D view. The FL1 phase has two separated Fermi surfaces with in-plane spin polarization cancels out after sum over all occupied states.

ization, and we call it the OP* phase [see Figs. 6 and 7] to distinguish it from the OP phase found in Ref. [49], which is shown in Fig. 3. The spin texture of the OP* phase is shown in Figs. 6 and 7. For large r_s , the right half of the phase diagram is the IP phase, shown in Fig. 8. A key feature of the IP phase is that the spin polarization is completely in plane. The IP phase gains exchange energy through the finite polarization, and the Fermi surface is shifted. MC simulations are roughly consistent with the analytical results in Sec. II, except for the appearance of the OP* phase. Another feature we have observed, and which is so not so easy to understand, is the extremely small energy difference between the PSH and the OP* states. We show in Fig. 9 a typical example. To interpret the results from our MC simulation, we choose a small enough spin-orbit parameter $\tilde{\alpha} = 0.16$ and different

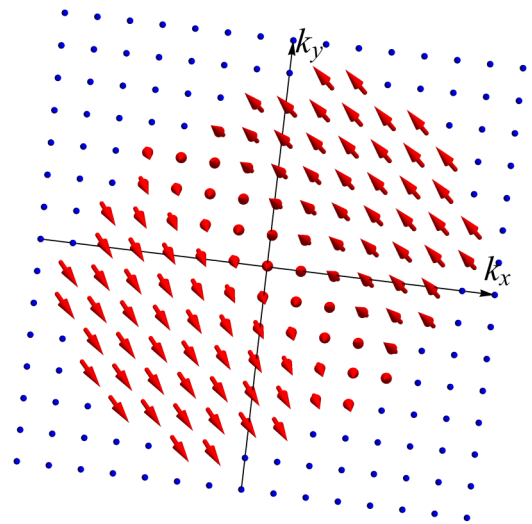


FIG. 6. The OP* state at $\tilde{\alpha} = \tilde{\beta} = 0.45$, $r_s = 2.10$ in a 3D view. The OP* phase has out-of-plane spin polarization, and the in-plane spin polarization cancels after sum over all occupied states.

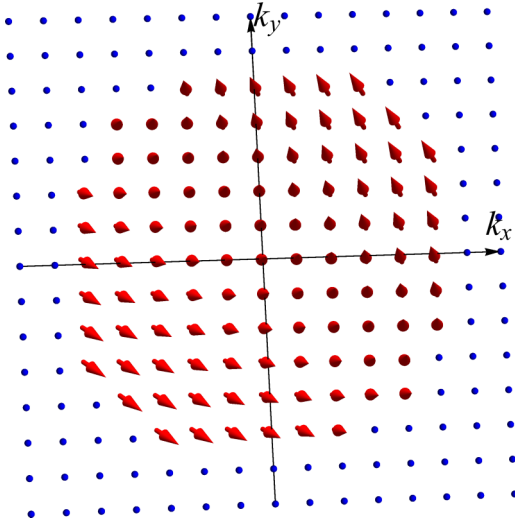


FIG. 7. The OP* state at $\tilde{\alpha} = 0.23$, $\tilde{\beta} = 0.23$, $r_s = 2.05$ in a 3D view. Compared with Fig. 6 with decreasing the SOC strength, the out-of-plane spin polarization becomes larger, and the Fermi surface is more compacted.

ratios $\tilde{\beta}/\tilde{\alpha}$ to determine the transition points, which are shown in Table I. From Table I, we see that the OP* region shrinks with increasing ratio $\tilde{\beta}/\tilde{\alpha}$. Although one possible interpretation is that the narrow region where the OP* phase is the ground state survives when $\tilde{\beta}/\tilde{\alpha} \rightarrow 1$, the discretization error of the k space is actually of the same order as the energy difference between the OP* phase and the IP phase. Therefore, despite the large value of $N = 997$, the classical MC simulation is not sensitive enough to do more than indicate the trend of the phase boundary between the OP* and the IP states. To perform a more careful finite-size scaling analysis, we extrapolate the energy difference of Fig. 9 to the thermodynamic limit ($N \rightarrow \infty$) and find that the IP phase has lower energy than the OP* phase. This indicates that, when $r_s > 2.01$, the

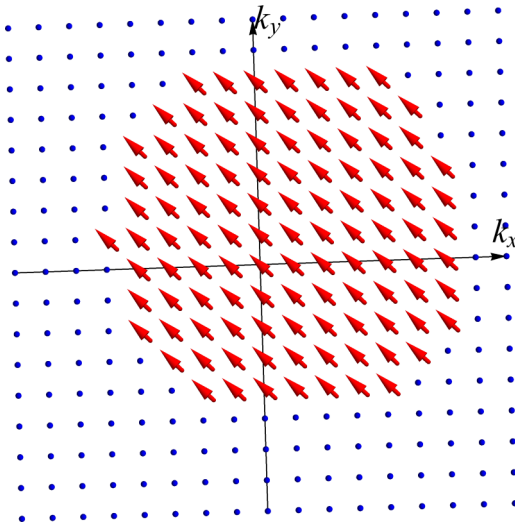


FIG. 8. The IP state at $\tilde{\alpha} = 0.23$, $\tilde{\beta} = 0.23$, $r_s = 2.30$ in a 3D view. The Fermi surface of the IP state with completely in-plane spin polarization is shifted along the $\frac{\pi}{4}$ direction.

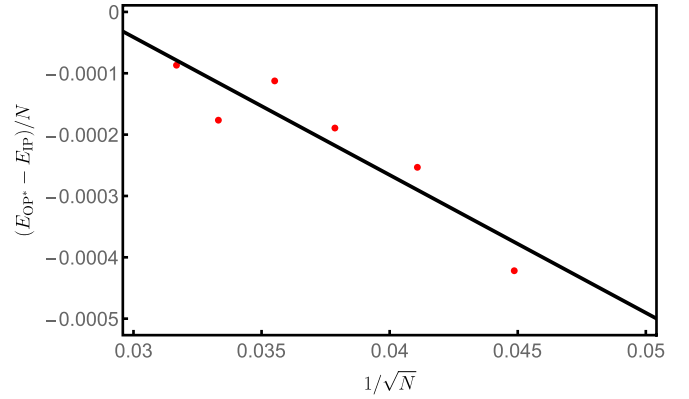


FIG. 9. Linear fit to find the ground state at $\tilde{\alpha} = \tilde{\beta} = 0.08$, $r_s = 2.10$, where N is the lattice number we take in the MC simulation.

ground state is the IP phase, bringing the numerical results in agreement with Fig. 1.

We finally comment about a possible origin of the OP* states. As we have already mentioned by construction our MC code does not capture spin-density-wave states. However, the SU(2) symmetry allows to transform the IP state to a family of spin-density waves [59,60] [see especially the arguments below Eq. (10) as well as Eq. (13)]. We believe that the OP* phase might be a remnant of the states with nonuniform spin polarization, thus, explaining the nearly degenerate energy with the IP state.

IV. EXPERIMENTAL VERIFICATION

A. Materials

The phase transitions presented in this paper occur as a function of electron-density r_s and the two parameters α and β that characterize the strengths of the Rashba and Dresselhaus interactions. In 2D systems r_s and α are tunable independently by means of the application of gate voltages and modulation doping. β is more usually thought of as an intrinsic parameter, but even it depends surprisingly strongly on the details of the interface and it may, therefore, ultimately be variable as well. Thus, the 2D case offers many advantages over the 3D case in the area of tunability. Indeed, despite many years of searching it is still somewhat unclear whether the ferromagnetism long predicted at low density in 3D has been observed, although there are some interesting experimental results along these lines Ref. [61].

In true 2D systems it may be difficult to obtain SOC strengths strong enough for the interesting effects postulated here to occur. The criterion is that the spin-orbit lengths $\hbar/m\alpha$ or $\hbar/m\beta$ should be comparable to the interelectron spacing.

TABLE I. The boundary with increasing ratio $\tilde{\beta}/\tilde{\alpha}$ where we choose $\tilde{\alpha} = 0.16$.

$\tilde{\beta}/\tilde{\alpha}$	FL2-OP/OP*	OP/OP* - IP
0	2.010	2.250
0.5	1.996	2.232
1	1.992	2.207

In Si and SiGe devices the spin-orbit coupling is simply too small. In GaAs, the Rashba spin-orbit lengths are around 10^{-7} m whereas typical devices have interparticle spacings perhaps a factor of 5 less than this. Working in this material probably the best way to observe the new phases in the near term. Indeed, there are indications of a spin-polarized state in 2D Si δ -doped GaAs/AlGaAs heterostructures [1].

Hole systems are also promising since the Rashba spin-orbit energy can be as large as 40% of the Fermi energy [62], and second-order effects in charge transport can be sizable [63]. The drawback in these systems is disorder. The mean free path ℓ tends to be short, and one certainly needs $k_F \ell \gg 1$ to observe anything.

Another intriguing possibility is the gas of surface states on topological insulators. These are the only systems where a one Fermi-surface state has actually been observed to date [3]. On the reverse side, disorder seems to be strong also in this case.

B. DC transport

In 2D electron systems transport measurements are always the the easiest to carry out. Since the various transitions that are envisioned here are first order, we expect discontinuous changes in both the longitudinal and the Hall resistances.

To have a finite resistance, we need to have disorder in the system. This begs the question of the stability of the different phases in the presence of disorder. We have not investigated this in any detail. However, the presence of SOC gives antilocalization at weak disorder strengths. This strongly suggests that the main effect of weak disorder would be to strengthen the role of the kinetic energy in its competition with the various forms of spin ordering. Thus, we might expect some downward renormalization of the interaction strength, but the ordered phases would remain stable.

The Boltzmann equation for electrical transport in 2D systems for arbitrary α and β and a simple scattering mechanism was solved by Schliemann and Loss for the FL2 states [64]. The coupled transport equations for both charge and spin have been written down [54], but have not yet found a detailed solution. Our purpose here is only to make predictions for qualitative changes across phase boundaries. Thus, we consider the linearized Boltzmann equation for a simple model of extreme short-range spin-preserving impurity scattering using the relaxation-time approximation. We will comment on other scattering mechanisms below. Furthermore, we estimate only the longitudinal resistance σ_{ij} with $i = j$ at zero magnetic field.

The conductivity is given by

$$\sigma_{ij} = \frac{e^2}{4\pi^2} \sum_{ns} \int d^2k \tau_{nks} v_{i,nks} v_{j,nks} \delta(E_{nks} - E_F). \quad (20)$$

Here n labels the pieces of the Fermi surface, k is the wave vector, E_{nks} is the energy, and τ_{nks} is the transport relaxation time of an electron with the indicated quantum numbers. The δ function pins the integrand to the Fermi surface. The i th component of the velocities $v_{i,nks}$ are the expectation values

of the operators,

$$\tilde{v}_x = p_x/m - \alpha\sigma_y + \beta\sigma_x, \quad (21)$$

$$\tilde{v}_y = p_y/m + \alpha\sigma_x - \beta\sigma_y. \quad (22)$$

The relaxation time is given by

$$\frac{1}{\tau_{nks}} = \frac{e^2}{4\pi^2} \sum_{n's'} \int d^2k' W_{nks,n'k's'} (1 - \cos \theta_{v(k),v(k')}). \quad (23)$$

$\theta_{v(k),v(k')}$ is the angle between the initial and the final velocities in a scattering process. Below, we will also use $\theta_{k,k'}$, the corresponding angle between wave vectors.

For our model the transition rate is

$$\begin{aligned} W_{nks,n'k's'} &= \frac{2\pi}{\hbar} \delta(E_{nks} - E_{n'k's'}) |\langle nks | U | n'k's' \rangle|^2 \\ &= \frac{2\pi n_{\text{imp}} u^2}{\hbar} \delta(E_{nks} - E_{n'k's'}) |\langle nks | n'k's' \rangle|^2. \end{aligned} \quad (24)$$

Since the impurity potential U is pointlike, the matrix element u is independent of momentum transfer. The last, and very important, factor is the overlap of the spinors at k and k' . Note that u has dimensions of energy times length squared in our normalization.

The amplitude for scattering from k to k' is proportional to the square of the overlap of the spinors at k and k' . In a completely polarized ferromagnetic state this amplitude is unity and the relaxation time τ_f is independent of k ,

$$\frac{1}{\tau_f} = \frac{n_{\text{imp}} u^2 k_F}{\hbar^2 v_F}, \quad (25)$$

where k_F and v_F are the Fermi wave vector and the Fermi velocity. We use τ_f as a benchmark for the relaxation times of the various phases.

Because of the spin textures, $|\langle nks | U | n'k's' \rangle|^2$ has a non-trivial k -dependence. Furthermore, it is highly dependent on the value of β/α . Referring to Fig. 1 of Ref. [49], we see a strongly chiral pattern of spin directions around any Fermi surface but as $\beta/\alpha \rightarrow 1$, Fig. 4 shows that the spin approach a ferromagnetic completely parallel pattern.

In the FL1 state τ is also isotropic. However, the chiral spin texture puts the spin at k at a fixed angle from the direction of k . We have

$$\begin{aligned} \frac{1}{\tau(\text{FL1})} &= \frac{1}{4\pi^2} \int d^2k W_{nks,n'k's'} \\ &\times (1 - \cos \theta_{v(k),v(k')}) (1 + \cos \theta_{k,k'}) / 2. \end{aligned} \quad (26)$$

The $(1 + \cos \theta_{k,k'})/2$ factor is absent in the corresponding expression for τ_f . Performing the integral when $\beta = 0$ we find $1/\tau_f \approx 4/\tau(\text{FL1})$. This becomes an equality when the velocity is parallel to the wave vector. The suppression of backscattering in the FL1 state enhances the conductivity dramatically, but as β/α increases this enhancement decreases. The expression for $\tau(\text{FL2})$ is more complicated. The suppression of backscattering is still present for intraband scattering. However, the importance of interband scattering increases as α decreases, and the two Fermi surfaces become similar in size. In our model the amplitudes for interband and intraband scattering are the same. The interband scattering includes

significant changes in momentum, so it will suppress the conductivity. So although the FL2 state has a conductivity that is significantly enhanced over the ferromagnetic state we expect it to be less than that of the FL1 state. Again, as β/α increases, all of these differences get smaller.

The spin terms in the velocity mainly affect the magnitude of the velocity rather than its angle, and in the chiral textures considered in this paper the overall trend is always to reduce the magnitude.

To understand the transport signatures of the various transitions, we first note that since all transitions are first order, we expect that the electrical conductivity σ will have a discontinuous jump at the transition. Since the size of the jumps depends on the exact point in the phase diagram and the fact that the model we have chosen is highly simplified, we do not attempt a truly quantitative calculation here. However, the effect of a significant change in a spin texture on σ is large, or relative order unity, so it makes sense to discern the overall patterns of the changes in σ .

The FL phases have a chiral spin texture. Perfect backscattering is forbidden since the spin wave functions are orthogonal in spin space. Hence, σ is maximal in these phases.

The OP state is rather close to the completely polarized ferromagnetic state in its spin texture, differing in that on the Fermi surface the spin angle from the z axis is γ , and although chirality is present, it is much reduced. This leads to a finite but reduced amount of backscattering suppression. Thus, this phase is close to the low- σ ferromagnetic phase. More specifically, we have

$$\frac{1/\tau(\text{OP})}{1/\tau_f} \approx \cos^4(\gamma/2) + \sin^4(\gamma/2) - \cos^2(\gamma/2)\sin^2(\gamma/2). \quad (27)$$

and in the limit of small γ the right-hand side is $1 - 3\gamma^2/4 + O(\gamma^4)$. Again, for the OP spin texture the velocity and wave vector are parallel, and the main effect of the spin-orbit coupling is to give a downward renormalization of the *magnitude* of velocity. Thus, the OP state has a conductivity close to the completely polarized state, and the conductivity increases with γ .

The IP phase has a complex texture that is not easily expressed analytically. However, it is the most interesting in that it breaks rotational symmetry by virtue of the displacement of the Fermi surface. In fact, the conductivity is anisotropic: $\sigma_{xx} \neq \sigma_{yy}$ for the state in Fig. 4. For definiteness, say that the Fermi surface moves off center along the $[0,1]$ direction. At the same time a ferromagnetic moment in the $[-1, 0]$ direction develops. If α is small, the state is nearly completely spin polarized, and the conductance is low and nearly isotropic. As α increases, the conductivity increases and becomes anisotropic. For states with $k \parallel \pm \hat{y}$ backscattering is allowed, whereas for states with $k \parallel \pm \hat{x}$ it is suppressed. Hence, the conductivity in the x direction in real space is enhanced relative to the y direction. Overall for the IP phase: (1) the conductivity depends strongly on the spin-orbit coupling strength with anisotropy developing as α increases; (2) $\sigma_{xx} > \sigma_{yy}$; (3) the jump in conductivity on passing from the OP to the IP phase is small at low α and increases as α increases; (4) overall, the conductivity is intermediate between the FL and OP states.

These considerations are summarized in Table II.

TABLE II. Conductivity of different phases at $\beta = 0$.

Phase	FL1	FL2	OP	IP
Conductivity	Highest	High	Low	Medium
Anisotropic	No	No	No	Yes

When $\beta \neq 0$ but $\beta < \alpha$ the conductivities of the FL1 and FL2 phases are anisotropic as pointed out by Schliemann and Loss [64]. The increase in β tends to cancel the antiferromagnetic effects of the Rashba coupling which, in turn, are associated with increased backscattering. These effects are summarized in Table III.

When $\beta = \alpha$, the OP phase disappears. The other phases can be mapped into phases of the system without SOC. Hence, we expect no backscattering suppression and isotropic and equal conductivities for all three phases. The conclusions are summarized in Table IV.

By means of transport measurements it should, therefore, be possible not only to detect phase transitions, but also to identify precisely which phases are involved.

We have assumed that the scattering matrix element is independent of the wave-vector change. If we take the other limit in which small-angle scattering dominates, then suppression of backscattering is no longer the dominant effect of SOC and rather the reduction of magnitude of velocity becomes important. In experiments this would have the very important affect that as the temperature increases and phonon scattering dominates, the picture we have presented here would change dramatically. One would expect mainly a gradual decrease in conductivity in all phases as the SOC increases.

V. CONCLUSION

The competition among the kinetic, interaction, and spin-orbit contributions to the electronic energy produces a rich variety of phases in the parameter space of the relative strengths of these energies. When we add the dimension of the relative strength of Rashba and Dresselhaus couplings α and β , the presence of an additional symmetry when $\alpha = \beta$ adds to the fascination of this physical system. We treat the symmetric point performing a canonical transformation and add the information so obtained to our MC simulation within the HF approximation. When $\alpha \neq \beta$, we identified four distinct ground states: FL1, FL2, OP, and IP phases, but when the symmetric point is approached, then the OP phase gets squeezed out. When the condition $\alpha = \beta$ has been reached, the IP phase can be identified with a PSH phase where spin-density waves are stabilized by the combined effect of SOC and interactions. The various phases have different DC transport properties, which aids experimental identification.

TABLE III. Conductivity of different phases at $0 < \beta < \alpha$.

Phase	FL1	FL2	OP	IP
Conductivity	Highest	High	Low	Medium
Anisotropic	Yes	Yes	Yes	Yes

TABLE IV. Conductivity of different phases at $\beta = \alpha$.

Phase	FL1	FL2	PSH
Conductivity	Medium	Medium	Medium
Anisotropic	No	No	No

The focus in this paper has been on 2D electron liquids in semiconductor structures, but we expect that for electrons on the surface of topological insulators similar considerations will apply. Indeed, it may be easier to reach the regime of very strong spin-orbit coupling. On the other hand, it is often difficult to disentangle surface from bulk transport. However, one may be able to perform spin-resolved photoemission and observe textures directly, an option that is not usually available in true 2D systems.

The Coulomb correlation energy increases the effective mass and the absolute value of the correlation energy of the

unpolarized 2DEG ground state is greater than its polarized counterpart [4,17]. So even with the correlation energy taken into account, the unpolarized FL1 and FL2 phases still have lower energies than that of the PSH phase. With regard to the Pomeranchuk instability, it is an instability in the shape of the Fermi surface of a material with interacting fermions, causing Landau's Fermi-liquid theory to break down [65,66]. The changes in Fermi-surface topology that we observe in the simulations are due to the action of mean fields and this means that the resemblance to the Pomeranchuk instability is only superficial.

ACKNOWLEDGMENTS

This research was supported by the Australian Research Council Centre of Excellence in Future Low-Energy Electronics Technologies (Project No. CE170100039) and funded by the Australian Government.

-
- [1] A. Ghosh, C. J. B. Ford, M. Pepper, H. E. Beere, and D. A. Ritchie, *Phys. Rev. Lett.* **92**, 116601 (2004).
- [2] G. Bihlmayer, O. Rader, and R. Winkler, *New J. Phys.* **17**, 050202 (2015).
- [3] D. Hsieh, Y. Xia, L. Wray, D. Qian, A. Pal, J. H. Dil, J. Osterwalder, F. Meier, G. Bihlmayer, C. L. Kane, Y. S. Hor, R. J. Cava, and M. Z. Hasan, *Science* **323**, 919 (2009).
- [4] C. Attaccalite, S. Moroni, P. Gori-Giorgi, and G. B. Bachelet, *Phys. Rev. Lett.* **88**, 256601 (2002).
- [5] J. Schliemann, *Rev. Mod. Phys.* **89**, 011001 (2017).
- [6] J.-J. Zhu, D.-X. Yao, S.-C. Zhang, and K. Chang, *Phys. Rev. Lett.* **106**, 097201 (2011).
- [7] A. Shekhter, M. Khodas, and A. M. Finkel'stein, *Phys. Rev. B* **71**, 165329 (2005).
- [8] J. Quintanilla and A. J. Schofield, *Phys. Rev. B* **74**, 115126 (2006).
- [9] L. Fu, *Phys. Rev. Lett.* **115**, 026401 (2015).
- [10] E. Berg, M. S. Rudner, and S. A. Kivelson, *Phys. Rev. B* **85**, 035116 (2012).
- [11] B. Tanatar and D. M. Ceperley, *Phys. Rev. B* **39**, 5005 (1989).
- [12] L. Baguët, F. Delyon, B. Bernu, and M. Holzmann, *Phys. Rev. Lett.* **111**, 166402 (2013).
- [13] L. O. Juri and P. I. Tamborenea, *Phys. Rev. B* **77**, 233310 (2008).
- [14] B. Bernu, F. Delyon, M. Holzmann, and L. Baguët, *Phys. Rev. B* **84**, 115115 (2011).
- [15] N. D. Drummond and R. J. Needs, *Phys. Rev. Lett.* **102**, 126402 (2009).
- [16] P. G. Bolcatto, C. R. Proetto, and F. A. Reboredo, *Phys. Rev. B* **67**, 073304 (2003).
- [17] A. K. Rajagopal and J. C. Kimball, *Phys. Rev. B* **15**, 2819 (1977).
- [18] D. Ceperley, *Phys. Rev. B* **18**, 3126 (1978).
- [19] G. Ortiz, M. Harris, and P. Ballone, *Phys. Rev. Lett.* **82**, 5317 (1999).
- [20] M. W. C. Dharma-wardana and F. Perrot, *Phys. Rev. Lett.* **90**, 136601 (2003).
- [21] S. Datta and B. Das, *Appl. Phys. Lett.* **56**, 665 (1990).
- [22] I. Žutić, J. Fabian, and S. Das Sarma, *Rev. Mod. Phys.* **76**, 323 (2004).
- [23] J. Sinova, S. O. Valenzuela, J. Wunderlich, C. H. Back, and T. Jungwirth, *Rev. Mod. Phys.* **87**, 1213 (2015).
- [24] K. Shen, G. Vignale, and R. Raimondi, *Phys. Rev. Lett.* **112**, 096601 (2014).
- [25] J.-J. Zhu, K. Chang, R.-B. Liu, and H.-Q. Lin, *Phys. Rev. B* **81**, 113302 (2010).
- [26] S. Chesi and G. F. Giuliani, *Phys. Rev. B* **83**, 235309 (2011).
- [27] G.-H. Chen and M. E. Raikh, *Phys. Rev. B* **60**, 4826 (1999).
- [28] H. Yamase, V. Oganesyan, and W. Metzner, *Phys. Rev. B* **72**, 035114 (2005).
- [29] W. M. C. Foulkes, L. Mitas, R. J. Needs, and G. Rajagopal, *Rev. Mod. Phys.* **73**, 33 (2001).
- [30] V. V. Braguta, M. I. Katsnelson, A. Y. Kotov, and A. A. Nikolaev, *Phys. Rev. B* **94**, 205147 (2016).
- [31] D. M. Ceperley and B. J. Alder, *Phys. Rev. Lett.* **45**, 566 (1980).
- [32] A. Ambrosetti, F. Pederiva, E. Lipparini, and S. Gandolfi, *Phys. Rev. B* **80**, 125306 (2009).
- [33] S. Azadi and T. D. Kühne, *J. Chem. Phys.* **146**, 084503 (2017).
- [34] S. C. Kapfer and W. Krauth, *Phys. Rev. E* **94**, 031302(R) (2016).
- [35] K. Takai, K. Ido, T. Misawa, Y. Yamaji, and M. Imada, *J. Phys. Soc. Jpn.* **85**, 034601 (2016).
- [36] S. Tanaka and S. Ichimaru, *Phys. Rev. B* **39**, 1036 (1989).
- [37] D. Varsano, S. Moroni, and G. Senatore, *Europhys. Lett.* **53**, 348 (2001).
- [38] D. M. Ceperley, *Nature (London)* **397**, 386 (1999).
- [39] S. Maiti, V. Zyuzin, and D. L. Maslov, *Phys. Rev. B* **91**, 035106 (2015).
- [40] H.-H. Kung, S. Maiti, X. Wang, S.-W. Cheong, D. L. Maslov, and G. Blumberg, *Phys. Rev. Lett.* **119**, 136802 (2017).
- [41] R. E. I, *Sov. Phys. Solid State* **1**, 368 (1959).
- [42] B. Shojaei, P. J. J. O'Malley, J. Shabani, P. Roushan, B. D. Schultz, R. M. Lutchyn, C. Nayak, J. M. Martinis, and C. J. Palmström, *Phys. Rev. B* **93**, 075302 (2016).
- [43] J. B. Miller, D. M. Zumbühl, C. M. Marcus, Y. B. Lyanda-Geller, D. Goldhaber-Gordon, K. Campman, and A. C. Gossard, *Phys. Rev. Lett.* **90**, 076807 (2003).

- [44] J. P. Lu, J. B. Yau, S. P. Shukla, M. Shayegan, L. Wissinger, U. Rössler, and R. Winkler, *Phys. Rev. Lett.* **81**, 1282 (1998).
- [45] G. Dresselhaus, A. F. Kip, and C. Kittel, *Phys. Rev.* **95**, 568 (1954).
- [46] I. L. Aleiner and V. I. Fal'ko, *Phys. Rev. Lett.* **87**, 256801 (2001).
- [47] M. Valín-Rodríguez, A. Puente, L. Serra, and E. Lipparini, *Phys. Rev. B* **66**, 165302 (2002).
- [48] S. Chesi, G. Simion, and G. F. Giuliani, [arXiv:cond-mat/0702060](https://arxiv.org/abs/cond-mat/0702060).
- [49] W. E. Liu, S. Chesi, D. Webb, U. Zülicke, R. Winkler, R. Joynt, and D. Culcer, *Phys. Rev. B* **96**, 235425 (2017).
- [50] J. Capps, D. C. Marinescu, and A. Manolescu, *Phys. Rev. B* **91**, 165301 (2015).
- [51] M. P. Walser, C. Reichl, W. Wegscheider, and G. Salis, *Nat. Phys.* **8**, 757 (2012).
- [52] J. D. Koralek, C. P. Weber, J. Orenstein, B. A. Bernevig, S.-C. Zhang, S. Mack, and D. D. Awschalom, *Nature (London)* **458**, 610 (2009).
- [53] F. Dettwiler, J. Fu, S. Mack, P. J. Weigele, J. C. Egues, D. D. Awschalom, and D. M. Zumbühl, *Phys. Rev. X* **7**, 031010 (2017).
- [54] B. A. Bernevig, J. Orenstein, and S.-C. Zhang, *Phys. Rev. Lett.* **97**, 236601 (2006).
- [55] M. Kohda, V. Lechner, Y. Kunihashi, T. Dollinger, P. Olbrich, C. Schönhuber, I. Caspers, V. V. Bel'kov, L. E. Golub, D. Weiss, K. Richter, J. Nitta, and S. D. Ganichev, *Phys. Rev. B* **86**, 081306(R) (2012).
- [56] B. Halperin, *J. Stat. Phys.* **175**, 521 (2019).
- [57] A. Schliemann, L. Worschech, S. Reitzenstein, S. Kaiser, and A. Forchel, *Phys. Status Solidi (c)* **1343** (2003).
- [58] G. F. Giuliani and G. Vignale, *Quantum Theory of the Electron Liquid* (Cambridge University Press, Cambridge, UK, 2005).
- [59] S. Kurth and F. G. Eich, *Phys. Rev. B* **80**, 125120 (2009).
- [60] K. S. Mosoyan, A. V. Rozhkov, A. O. Sboychakov, and A. L. Rakhmanov, *Phys. Rev. B* **97**, 075131 (2018).
- [61] D. P. Young, D. Hall, M. E. Torelli, Z. Fisk, J. L. Sarrao, J. D. Thompson, H.-R. Ott, S. B. Oseroff, R. G. Goodrich, and R. Zysler, *Nature (London)* **397**, 412 (1999).
- [62] E. Marcellina, A. R. Hamilton, R. Winkler, and D. Culcer, *Phys. Rev. B* **95**, 075305 (2017).
- [63] H. Liu, E. Marcellina, A. R. Hamilton, and D. Culcer, *Phys. Rev. Lett.* **121**, 087701 (2018).
- [64] J. Schliemann and D. Loss, *Phys. Rev. B* **68**, 165311 (2003).
- [65] I. I. Pomeranchuk, *Sov. Phys. JETP* **8**, 361 (1958).
- [66] J. Quintanilla, C. Hooley, B. Powell, A. Schofield, and M. Haque, *Physica B* **403**, 1279 (2008).